ISSCR

OCIAD1 Controls Electron Transport Chain Complex I Activity to Regulate Energy Metabolism in Human Pluripotent Stem Cells

Deeti K. Shetty,[1] Kaustubh P. Kalamkar,[1] and Maneesha S. Inamdar[1,2,*]

[1]Jawaharlal Nehru Centre for Advanced Scientific Research, Bengaluru 560064, India
[2]Institute for Stem Cell Biology and Regenerative Medicine, Bengaluru 560065, India
*Correspondence: inamdar@jncasr.ac.in
https://doi.org/10.1016/j.stemcr.2018.05.015

SUMMARY

Pluripotent stem cells (PSCs) derive energy predominantly from glycolysis and not the energy-efficient oxidative phosphorylation (OXPHOS). Differentiation is initiated with energy metabolic shift from glycolysis to OXPHOS. We investigated the role of mitochondrial energy metabolism in human PSCs using molecular, biochemical, genetic, and pharmacological approaches. We show that the carcinoma protein OCIAD1 interacts with and regulates mitochondrial complex I activity. Energy metabolic assays on live pluripotent cells showed that OCIAD1-depleted cells have increased OXPHOS and may be poised for differentiation. OCIAD1 maintains human embryonic stem cells, and its depletion by CRISPR/Cas9-mediated knockout leads to rapid and increased differentiation upon induction, whereas OCIAD1 overexpression has the opposite effect. Pharmacological alteration of complex I activity was able to rescue the defects of OCIAD1 modulation. Thus, hPSCs can exist in energy metabolic substates. OCIAD1 provides a target to screen for additional modulators of mitochondrial activity to promote transient multipotent precursor expansion or enhance differentiation.

INTRODUCTION

The dual capacity of self-renewal and multipotent differentiation that is unique to stem cells has opened new vistas for cell therapy and regenerative medicine with great therapeutic promise (Ito and Suda, 2014). Adult stem cells or intermediate precursor populations allow faster and efficient generation of desired lineages than pluripotent stem cells (PSCs) (Kumar et al., 2015). However, the rate of self-renewal declines with age, resulting in stem cell exhaustion. Hence a deeper understanding of mechanisms that regulate PSC self-renewal and differentiation would help in devising new strategies and culture systems to expand desired multipotent intermediates in a safe and accessible manner.

Human PSCs rely on glycolysis for their energy requirements, whereas differentiated derivatives have progressively increasing oxidative phosphorylation activity (Ito and Suda, 2014; Varum et al., 2011). Identifying regulators of the changing energy metabolic state during stem cell differentiation could lead to new strategies for expansion of desired stem or precursor cells and suggest non-genetic means to transiently expand them while avoiding potential malignant transformation, thus making it more suitable for therapeutic application. With this aim we chose to analyze the human carcinoma protein ovarian carcinoma immunoreactive antigen domain containing-1 (OCIAD1) for its normal role in PSC differentiation.

Human OCIAD1 is misexpressed in several carcinomas (De Marchi et al., 2016; Sengupta et al., 2008; Yang et al., 2012); however, its normal expression and function are not known. During mouse development, OCIAD1/Asrij is

expressed in early embryonic mesoderm and cardiovascular lineages. The protein localizes to endosomal compartments (Kulkarni et al., 2011; Mukhopadhyay et al., 2003) and mitochondria (Mouse MitoCarta2.0 [Calvo et al., 2015; Pagliarini et al., 2008]) and regulates multiple signaling pathways such as JAK/STAT, Notch, and PI3K/AKT to regulate cell fate (Kulkarni et al., 2011; Sinha et al., 2013). Asrij is essential for maintaining mouse embryonic stem cell (mESC) pluripotency as well as *Drosophila* hematopoietic stem cells. In both systems Asrij overexpression maintains stemness and its depletion leads to precocious differentiation of mouse pluripotent cells or *Drosophila* blood cells (Khadilkar et al., 2014; Kulkarni et al., 2011; Sinha et al., 2013).

To test the role of human OCIAD1 in stem cells and early development, we used human embryonic stem cells (hESCs) as a model. Earlier studies showed that reduced or increased expression of OCIAD1 in hESCs does not affect their morphology, pluripotency marker gene expression, or ability to differentiate to derivatives of ectoderm, mesoderm, and endoderm (Shetty and Inamdar, 2016a, 2016b, 2016c). Using genetically modulated *OCIAD1* hESCs or pharmacological enhancement of OCIAD1 expression, we show that OCIAD1 regulates energy metabolism of hESCs through mitochondrial complex I activity. Using mesoderm differentiation as a model, we show that the energy metabolic state affects PSC potency for differentiation. Furthermore, pharmacological modulation of mitochondrial complex I activity showed similar effects with hESCs. Thus, using OCIAD1 and mesoderm differentiation as tools, we show that the energy metabolic state of PSCs determines their response to differentiation cues.

We propose that OCIAD1 provides a target to screen for efficient and specific modulators of energy metabolic activity that will find wide application in understanding stem cell biology, aging, and cancer.

RESULTS

OCIAD1 Is Expressed in Human Pluripotent Stem Cells

We showed previously that mouse Asrij/OCIAD1 is expressed in early mesoderm and is essential for mESC pluripotency. Immunolocalization and RT-PCR analysis in hESC lines BJNhem19 and BJNhem20 (Inamdar et al., 2009; International Stem Cell Initiative et al., 2011; Venu et al., 2010) showed that OCIAD1 is expressed in undifferentiated hESCs that express pluripotency markers (at the protein level [Figure S1A] and the transcript level [Figure S1B]). Western blot analysis of hESC lysates revealed a protein of 34 kDa (Figure S1C). To assess the role of OCIAD1, we generated hESC lines that expressed exogenous OCIAD1 (OV, for overexpressed) (Shetty and Inamdar, 2016c) or had reduced OCIAD1 expression due to CRISPR/Cas9-mediated deletion in exon 3 resulting in a truncated protein of 51 amino acids and, hence, a heterozygous knockout line (Het-KO). Change in OCIAD1 levels had no apparent effect on colony morphology, pluripotency marker expression, and ability to differentiate to derivatives of all three germ layers in spontaneously differentiated embryoid bodies (Shetty and Inamdar, 2016a, 2016b, 2016c) (Figures S2A–S2C). We used two Het-KO hESC lines harboring two different mutations in *OCIAD1* (CRISPR-20 and CRISPR-39) and since both yielded similar results, all further studies analyzed Het-KO[CRISPR-39] as the level of OCIAD1 expression was lower in this line from the normal allele.

OCIAD1 Is a Mitochondrial Protein and Interacts with the Electron Transport Chain

To investigate how OCIAD1 may regulate stem cell differentiation, we examined its subcellular location by immunofluorescence analysis with anti-OCIAD1 antibodies. Wild-type (WT) hESCs showed a punctate pattern, and co-localization analysis with various organelle markers (Figures S3A–S3E) showed that OCIAD1 resides predominantly in mitochondria in hESCs (Figures 1A and S3A–S3E) as in other human cells (Calvo et al., 2015; Pagliarini et al., 2008). High-throughput affinity-capture mass spectrometry-based interactions for OCIAD1 were reported with several mitochondrial proteins of the inner mitochondrial membrane (IMM) including TIMMDC1, NDUFS2, COX6A1, and SDHB (Floyd et al., 2016; Guarani et al., 2014; Havugimana et al., 2012). A proximity ligation assay (PLA) for OCIAD1 and NDUFS3, an IMM pro-

tein, or MIC60 (a member of mitochondrial contact site and cristae organizing system) indicated that OCIAD1 associates with the IMM (Figure 1B). Furthermore, immunoprecipitation from WT hESC lysates and probing for representative members of each ETC complex showed that OCIAD1 interacts with members of complex I (TIMMDC1, NDUFS3), complex IV (CoxIV), and complex V (ATP5a) but not with the reported interactor from complex II (SDHB) or the complex III representative (UQCRC2) in hESCs (Figure 1C).

OCIAD1 Regulates ETC Complex I Activity

We next tested for a possible role of OCIAD1 in regulating mitochondrial activity. WT, OV, and Het-KO hESCs grown under conditions that maintain pluripotency were processed appropriately and assayed for the activity of individual ETC complexes (see Experimental Procedures). Mitochondrial abundance was assessed by the activity of citrate synthase and found to be comparable across the three lines (Figure 1D).

Complex I (NADH:ubiquinone oxidoreductase) oxidizes NADH, facilitating entry of electrons into the ETC, and contributes to the proton gradient and reactive oxygen species (ROS) production. Complex I activity correlated inversely with OCIAD1 expression: overexpression decreased the activity by 2-fold whereas OCIAD1 reduction caused a 2.5-fold increase in activity (Figure 1E). The path of electron flow originates at NADH oxidation by complex I and is routed through complexes III to IV. Complex III (coenzyme Q-cytochrome *c* reductase) activity was not significantly altered across OCIAD1-modulated conditions (Figure 1F). Complex IV (cytochrome *c* oxidase) transfers electrons to the terminal electron acceptor, i.e., molecular oxygen, and oxidizes cytochrome *c*. OCIAD1 modulation resulted in a small change in this enzymatic activity of about 1.25-fold (Figure 1G).

OCIAD1 regulates complex I activity, which is a major contributor of ROS. Staining for MitoSOX red showed that while mitochondrial ROS levels in OV were comparable with those of WT cells, Het-KO ROS levels increased by 1.487-fold, probably owing to high complex I activity (Figure S4A). Furthermore, OV had reduced transcript levels of antioxidant enzyme *superoxide dismutase 2* (*SOD2*) while Het-KO had almost 2-fold higher expression (Figure S4B), which could be a response to increased ROS levels. Increased *SOD2* may contribute to control of steady-state ROS levels, giving the cells a survival advantage when the culture differentiates. ROS functions as a signaling molecule to aid differentiation of stem cells and does not cause any detrimental effects on the mitochondria at low steady-state levels; rather, these levels are indicative of normal function of mitochondrial metabolism (Maraldi et al., 2015).
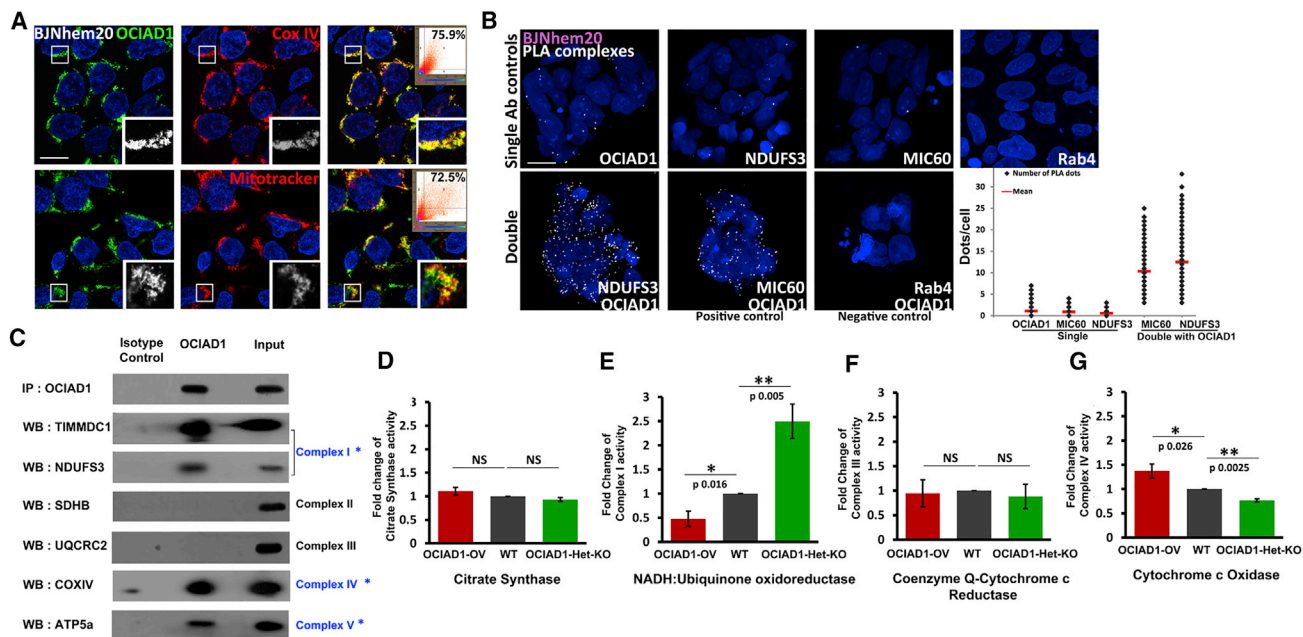
Figure 1. OCIAD1 Interacts with Mitochondrial ETC Complexes I, IV, and V in hESCs and Regulates Complex I Activity

(A–C) Wild-type (WT) hESCs were analyzed for subcellular localization of OCIAD1 and interaction with mitochondrial ETC proteins.

(A) Immunostaining of hESC cultures for OCIAD1 (green) and mitochondrial markers (red) COXIV or MitoTracker. Inset scatterplots show co-localizing pixels and percent co-localization analyzed for a single slice (N = 3, n > 50 cells). Scale bar, 100 μm.

(B) *In situ* PLA demonstrating the interaction between OCIAD1 and NDUFS3, or OCIAD1 and MIC60 in hESCs, seen as white dots. Single antibody controls as well as OCIAD1 with Rab4 (negative control) had less or no PLA complexes. Graph represents PLA complex dots/cell (n = 100 cells). DAPI-stained nuclei are in blue. Scale bar, 100 μm.

(C) Immuno-pull-down of endogenous OCIAD1 from hESC cultures followed by western blot (WB) analysis to probe for interaction with representative interacting proteins from ETC complexes I–V as indicated. Beads bound with rabbit immunoglobulin G isotype control were taken as negative control and input lysate as a positive control (N = 3).

(D–G) WT, OCIAD1-overexpressing (OV), and OCIAD1-depleted (Het-KO) hESCs were analyzed in the undifferentiated state for activity of ETC enzymes citrate synthase (D), NADH:ubiquinone oxidoreductase (E), coenzyme Q-cytochrome *c* reductase (F), and cytochrome *c* oxidase (G). Complex I activity was determined by monitoring the decrease in NADH absorbance at 350 nm, in the presence or absence of inhibitor rotenone. Similarly, activities of complexes III and IV were determined by assaying for reduction and oxidation of cytochrome *c*, respectively, using inhibitors antimycin A or sodium azide, respectively. Slopes of the curves of OD are calculated and normalized for protein content, and the enzymatic activities are computed in the presence and absence of inhibitor. Only fold change in enzymatic activity is represented here for simplicity, depicted across the WT and OCIAD1 modulated hESCs. Statistical significance is indicated by *p < 0.05 and **p < 0.01; NS, not significant. Error bars show SEM.

In summary, OCIAD1 primarily controls complex I activity, but minor changes in complex IV activity may also contribute to overall OXPHOS activity. Complex IV/cytochrome *c* oxidase activity is required for assembly and stability of complex I in fibroblasts (Li et al., 2006). However, the role in PSCs is not known. To assess the overall effect of changes in ETC complex activities and gain insight into its biological relevance, we profiled live OCIAD1-modulated hESCs for their energy metabolic state.

OCIAD1 Modulation Alters Energy Metabolic Profile of hESCs

It is known that hPSCs are less dependent on OXPHOS for energy production and rely more on glycolysis. Differ-

entiation of hPSCs is correlated with glycolytic to OXPHOS switch in terms of energy dependence. The Mitostress profiling of hPSCs shows a greater reduction in oxygen consumption upon oligomycin A (an inhibitor of ATP synthase activity) treatment compared with differentiated fibroblast cells, suggesting that hPSCs are less dependent than fibroblasts on OXPHOS. Furthermore, hPSCs respire at their maximal capacity and lack spare respiratory capacity. On the other hand, differentiated cells are able to increase oxygen consumption in order to produce more ATP (Varum et al., 2009; Zhang et al., 2011).

Undifferentiated WT, OV, and Het-KO hESCs were profiled for oxygen consumption rate (OCR), a readout of
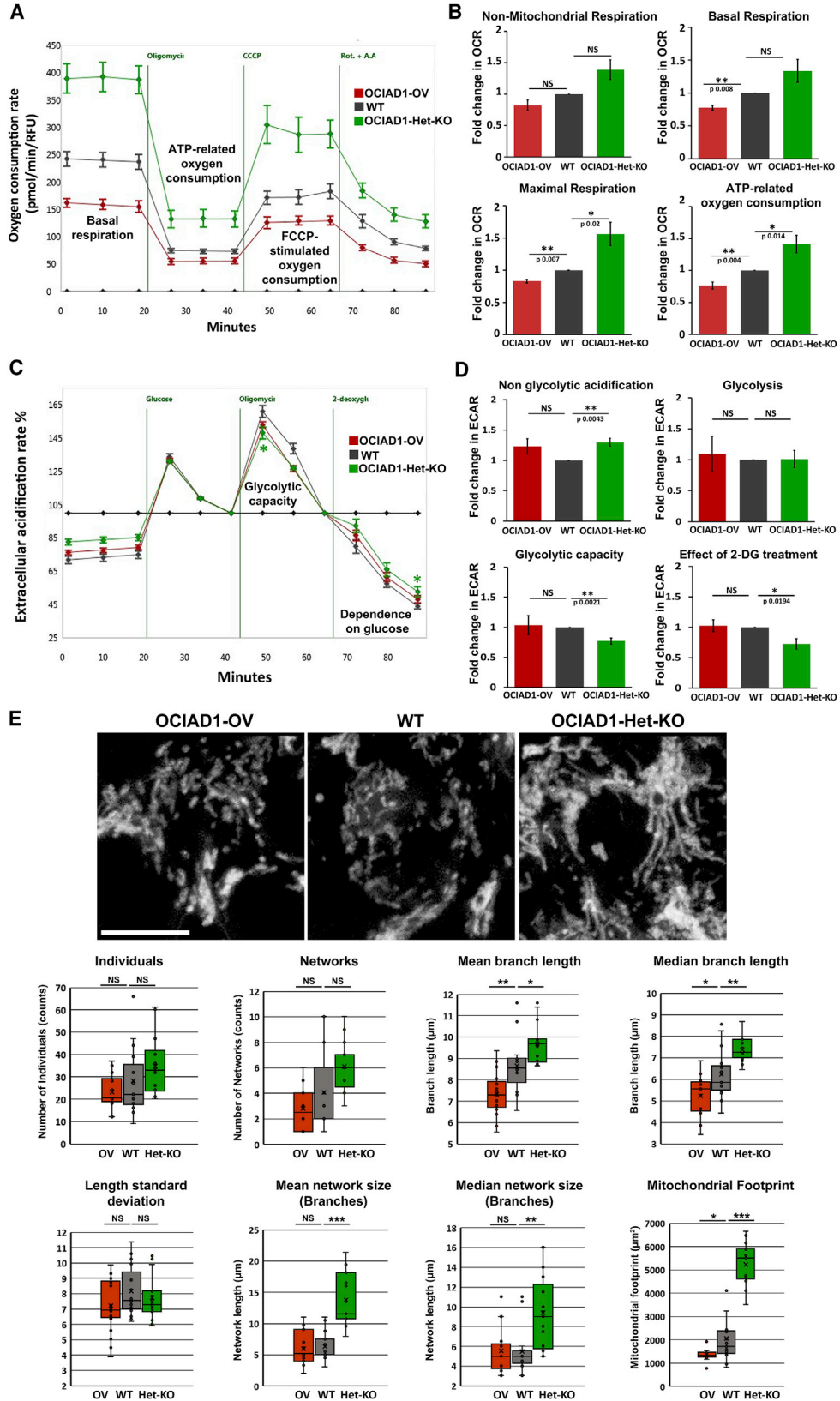
(legend on next page)

the OXPHOS status (see Experimental Procedures). Bioenergetic profiling by the Mitostress assay revealed that OCIAD1 overexpression caused reduction in the basal respiration and carbonyl cyanide-4-(trifluoromethoxy) phenylhydrazone (FCCP)-stimulated rate (at 0.3 μM) of hESCs (Figures 2A and 2B). True maximal respiration was not determined. Oligomycin-inhibited rate indicates the amount of non-phosphorylating respiration. Oligomycin A treatment of OV cells reduced the ATP-related oxygen consumption to less than in WT, indicating that a lower proportion of the total respiration is for ATP generation. A smaller difference between FCCP-stimulated rate and oligomycin-inhibited rate suggested that the relative amount of respiratory chain uncoupling of OV cells could be more than of WT. Thus, the bioenergetic profile of OV resembles that of undifferentiated stem cells. In contrast, Het-KO had high FCCP-stimulated rate (at 0.3 μM) and increased ATP-related oxygen consumption. Thus, although they express markers of pluripotency (Figures 3E and 3F), Het-KO hESCs have a greater capacity to consume oxygen than WT. Het-KO showed a larger drop in ATP-related oxygen consumption upon oligomycin treatment as compared with WT (Figures 2A and 2B). A greater reduction of the oligomycin-inhibited rate indicates a higher proportion of the total respiration is for ATP generation. A larger difference between FCCP-stimulated rate and oligomycin-inhibited rate suggested that the relative amount of respiratory chain uncoupling of Het-KO cells could be less than WT. Thus, reduction in OCIAD1 levels changes the energy metabolic profile toward differentiation; however, the change is not as drastic as that of a differentiated cell (Varum et al., 2009) (Zhang et al., 2011), hence the hESCs retain pluripotent characteristics.

Glycolysis levels were quantified by the Glycostress assay, which gives extracellular acidic flux/rate (ECAR), a readout of the extent of glycolysis. ECAR profiling provides a measure of parameters such as non-glycolytic acidification, glycolytic capacity and ECAR reduction upon 2-deoxyglucose (2-DG) (a competitive structural analog of glucose) addition. As hPSCs rely primarily on glycolysis for energy production, 2-DG addition to the medium causes a greater decline in ECAR (65%) compared with that of a differentiated cell (45%), as PSCs are more dependent on glycolysis for energy (Zhang et al., 2011). There was no significant change in most of the functional parameters of glycolysis in OV hESC compared with WT, suggesting that metabolically they resemble hPSCs (Figures 2C and 2D). However, Het-KO had reduced glycolytic capacity and lower dependence on glucose for energy generation (Figures 2C and 2D). Thus, though undifferentiated by standard analyses, Het-KO hESCs may have shifted their metabolic profile from glycolysis toward more oxygen consumption for ATP generation in the undifferentiated state (Figures 2A–2D). Reducing OCIAD1 levels probably makes cells unable to sustain only through glycolysis and nudges them toward oxidative phosphorylation-based energy metabolism. These Het-KO cells may be poised to differentiate as an outcome of increased mitochondrial elongation, in addition to changes in respiration. Hence, we assayed for changes in mitochondrial morphology and differentiation in OCIAD1-modulated cells.

Mitochondrial Morphology Correlates with OXPHOS Status in OCIAD1-Modulated Cells

Mitochondrial elongation and maturation by forming more cristae allows assembly of ETC subunits for active OXPHOS (Wanet et al., 2015; Xu et al., 2013). MitoTracker

Figure 2. OCIAD1 Modulation Alters Energy Metabolic Profile of hESCs Supported by Changes in Mitochondrial Morphology

(A–D) Bioenergetic profiling using Seahorse bioanalyzer of undifferentiated wild-type (WT), OCIAD1-overexpressing (OV), and OCIAD1-depleted (Het-KO) hESCs.

(A) Plot representing oxygen consumption rate (OCR) versus time (min) upon sequential injection of mitochondrial ETC function inhibitor oligomycin (1 μM), FCCP (protonophore) (0.3 μM), and inhibitors rotenone and antimycin A (at 1 μM each). Error bars show SEM for N = 4, n = 3.

(B) Graphical representation of fold changes relative to WT for various parameters listed, as indicated upon OCR analysis. Non-mitochondrial respiration is minimum rate measured after rotenone + antimycin A treatment. Basal respiration is the (rate before oligomycin induction) – (non-mitochondrial respiration). Maximal respiration indicates (FCCP-stimulated rate at 0.3 μM) – (oligomycin-inhibited rate). Note that true maximal rate was not determined. ATP-related oxygen consumption is (basal respiration) – (oligomycin-inhibited rate).

(C) Plot of extracellular acidification rate (ECAR) percent change versus time (min) upon sequential injection of glucose (25 μM), oligomycin (1 μM), and 2-deoxyglucose (25 μM). Baselines were set to 100% at the time points of oligomycin and 2-DG addition.

(D) Graphical representation of fold changes relative to WT for various parameters upon ECAR analysis. Error bars show SEM for N = 3 with n = 3 for OV and Het-KO hESCs.

(E) 3D projected fluorescence imaging of MitoTracker deep red-stained OCIAD1-modulated hESCs. Mitochondrial network analysis parameters were computed for over 375 mitochondria per genotype from at least 20 cells (see Supplemental Experimental Procedures). Error bars show SD. Scale bar, 10 μm.

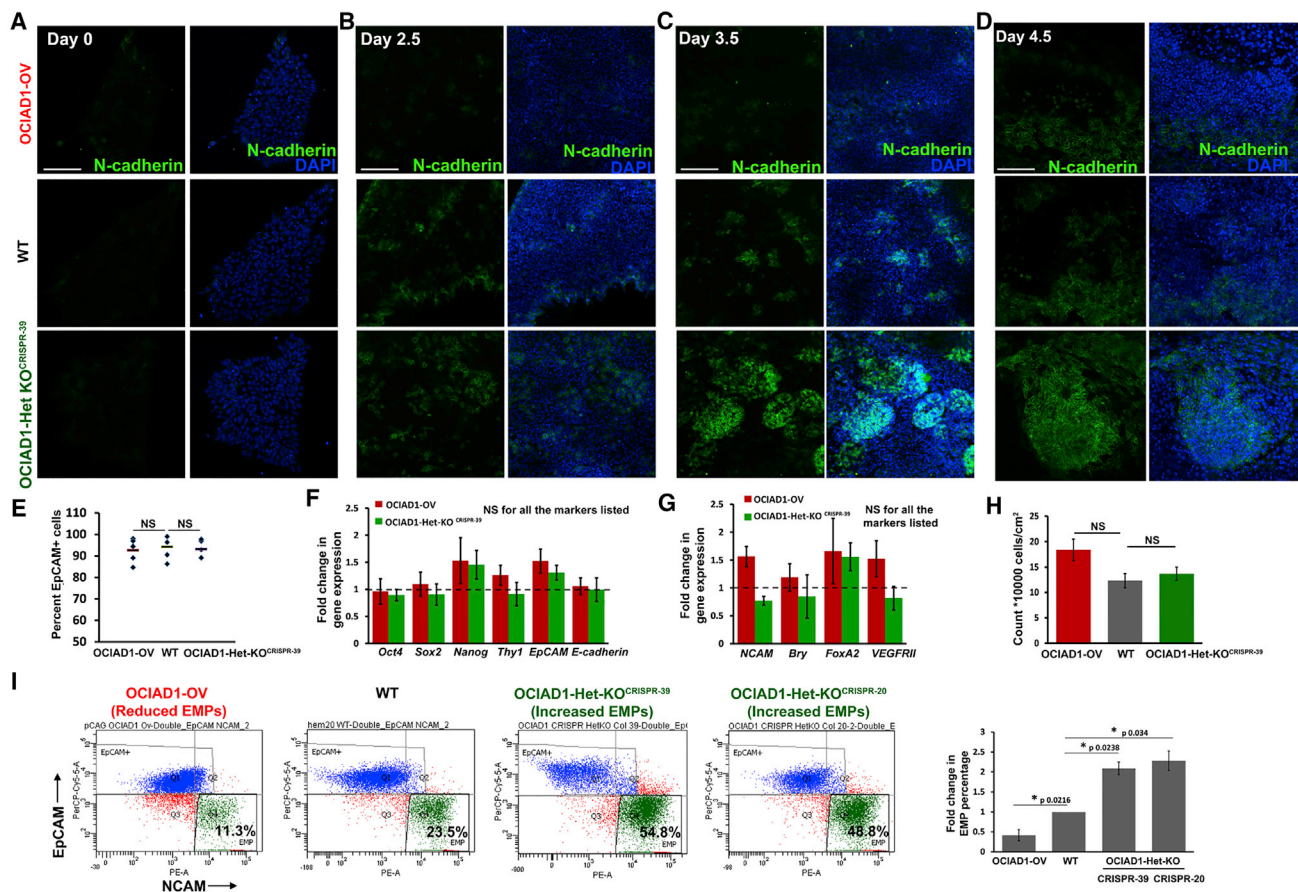*p < 0.05, **p < 0.01, ***p < 0.001; NS, not significant.

Figure 3. OCIAD1 Regulates Early Mesoderm Progenitor Formation

(A–H) Wild-type (WT), OCIAD1-overexpressing (OV), and OCIAD1-depleted (Het-KO) hESCs were analyzed in the undifferentiated state (A and D–G) or at various days of directed mesoderm differentiation as indicated (B–D and H). Het-KO cells used were Het-KO[CRISPR-39] or Het-KO[CRISPR-20] clone as indicated. (A–D) Immunostaining of cultures at day 0, 2.5, 3.5, or 4.5 to show expression and distribution of N-cadherin+ cells in the culture indicating epithelial-to-mesenchymal transition. Nuclei are marked by DAPI (blue) (N = 3). Scale bars, 100 μm. (E) Flow-cytometry analysis of cultures at day 0 of differentiation showing the percentage of EpCAM+ cells. N = 4. (E and F) qRT-PCR analysis of pluripotency gene expression (F) or EMT and mesendodermal marker gene expression (G) in cultures at day 0 is shown as fold change in gene expression as compared with WT (dotted line). (H) Viable cell counts based on trypan blue exclusion staining of hESC cultures at day 0 over four consecutive passages (biological replicates N = 4, technical replicates n = 2).

(I) Flow-cytometric analysis of EpCAM− NCAM+ cells (EMPs) at day 4.5 of differentiation across various genotypes as indicated. Representative scatterplots from one experiment show the distribution of cells in various quadrants, and percent EMP is indicated. Graph shows quantitation as fold change in percentage of EMPs (N > 5).

Error bars show SEM. *p < 0.05; NS, not significant.

labeling and live confocal imaging of OCIAD1-modulated hESCs along with 3D projection was performed for morphological analysis (Figure 2E and Video S1) (see Supplemental Experimental Procedures). Based on mean and median branch lengths, OV cells had a higher proportion of short mitochondria compared with WT, and Het-KO had more of elongated mitochondria. Furthermore, the mitochondria of Het-KO were arranged as longer networks, resembling cells initiating differentiation. However, since the cultures were undifferentiated, we propose that mitochondrial morphology seen is indicative of their

propensity to differentiate. The area occupied by mitochondrial structures within a cell (mitochondrial footprint) was also inversely correlated to OCIAD1 expression (Figure 2E).

Change in mitochondrial morphology could be a cause or outcome of changes in ETC activity. As OCIAD1 interacts with MIC60, which maintains cristae junctions, inner membrane architecture, and forms contact sites to the outer membrane, it could have pleiotropic roles in maintenance of naive or immature state of mitochondria, which merits further investigation.

OCIAD1 Is Expressed During Mesoderm Differentiation

OCIAD1 is also called *emi2* as it is induced in mouse metanephric mesenchyme (Abidari et al., 2000). Hence, we analyzed its expression in mesodermal derivatives obtained by subjecting hESCs to a directed mesoderm differentiation protocol in the presence of activin A, BMP4, VEGF, and basic fibroblast growth factor (see Experimental Procedures and Figure S5A) whereby EpCAM$^+$ pluripotent cells which are epithelial-like are present at day 0, EpCAM$^-$ NCAM$^+$ early mesoderm progenitors (EMPs) appear from day 3.5 of differentiation, and hematoendothelial and mesenchymal lineages are seen by day 7.0. qRT-PCR analysis of mRNA showed that *OCIAD1* expression remained fairly constant through mesoderm differentiation (Figure S5B), while *NCAM* expression increased at day 3.5. Other markers of mesoderm lineages, namely, *VEGFRII* (hemangioblast/endothelial), *CD34* (hematopoietic), and *PDGFR-α* (mesenchyme), were detected at day 7 as expected (Figure S5B), indicating that the time line of differentiation was as reported previously (Evseenko et al., 2010). Immuno-localization analysis showed that E-cadherin associated with undifferentiated hESCs was expressed throughout the colony at day 0 (Figure S5C) but was limited to clusters at day 3.5 with concomitant increase in cells expressing indicators of the epithelial-to-mesenchymal transition (EMT), namely N-cadherin, vimentin, fibronectin, and Msx2 as well as the mesendodermal marker Brachyury (Figure S5D). Further analysis at day 7.0 after culture in appropriate media (see Experimental Procedures) showed the presence of endothelial cells, hematopoietic clusters, and mesenchymal cells in the culture (Figures S5E and S5F).

OCIAD1 Delays Human Early Mesodermal Progenitor Specification

As OCIAD1 is expressed throughout mesodermal differentiation (Figure S5B) and this process is enhanced by increasing ROS (Ji et al., 2010), we chose to test the role of OCIAD1 in hPSC by subjecting OCIAD1-modulated hESCs to directed mesoderm differentiation and analyzed for the appearance of EpCAM$^-$ NCAM$^+$ EMPs (Figures 3A–3D). WT cultures showed increasing N-cadherin$^+$ clusters from day 2.5 to day 4.5, indicating that EMT had been initiated. It should be noted that day 3.5 is the first time point of EMP generation reported (Evseenko et al., 2010). OV cells had relatively fewer N-cadherin$^+$ cells at days 2.5–4.5, but the number was increased greatly in Het-KO cultures, from day 2.5 of differentiation, a day earlier than in WT. Large areas of N-cadherin$^+$ cells were seen at day 2.5 and large N-cadherin$^+$ clusters at day 3.5, suggesting that EMT occurs earlier in OCIAD1-depleted conditions (Figures 3B and 3C).

To rule out the possibility that variation in the extent of EMT induction in the cultures is due to varying hESC numbers in the starting population, we analyzed the hESCs grown on Matrigel-coated dishes for expression of EpCAM by flow cytometry and found no significant differences in EpCAM$^+$ cell percentages between WT, OCIAD1-OV, and OCIAD1-Het-KO hESCs (Figure 3E) and also the mean fluorescence intensity of EpCAM expression across the lines (Figure S2C). qRT-PCR analysis of transcripts for pluripotency marker genes (*Oct4*, *Sox2*, *Nanog*, *Thy1*, *EpCAM*, *E-cadherin*) in day-0 cultures also showed no significant difference in expression levels between the three lines (Figure 3F). Furthermore, in the undifferentiated state there was no significant difference in the transcript levels of EMT and mesodermal markers of early differentiation (Figure 3G). Proliferation of OCIAD1-modulated cells was also comparable with that of WT (Figure 3H).

The EMP population (EpCAM$^-$ NCAM$^+$) in mesoderm-induced cultures was analyzed by flow cytometry of live cells stained for the cell surface markers EpCAM and NCAM. Since sufficient EMPs were generated by day 4.5 across the three hESC lines, as observed by qualitative analysis (Figure 3D) and due to the increase in EMP population by day 4.5 compared with day 3.5 of induction in WT cultures (see Figure S5G), this time point was chosen for quantitative analysis by flow cytometry. Compared with WT (23.5%), OV cells generated fewer EMPs by day 4.5 (11.3%), whereas Het-KO cells had double the percentage of EMPs (54.8% for Het-KO$^{CRISPR-39}$ and 48.8% for Het-KO$^{CRISPR-20}$) (Figure 3I). Thus, increased levels of OCIAD1 delay differentiation whereas reduced OCIAD1 levels favor differentiation, suggesting that OCIAD1 may regulate the specification of EMPs.

To test the potency of generated EMPs in the mutant lines, we differentiated them further and analyzed generation of mesenchyme and hematoendothelial lineages. There was no significant change in the percentage of CD73$^+$ mesenchymal cells generated (Figures S6A and S6B). However, VEGFRII$^+$ and CD34$^+$ cells were low in OV cultures and relatively high in Het-KO, as compared with WT (Figures S6C and S6D), indicating that OCIAD1 may affect lineage differentiation too.

Thus, OCIAD1 regulates the propensity of pluripotent cells to differentiate. When OCIAD1 levels are low, though cells are pluripotent, they seem poised to differentiate and hence can respond rapidly to exogenous growth factors that promote mesoderm differentiation.

Pharmacological Enhancement of OCIAD1 Expression Reduces EMP Generation

Insight into the significant effect of OCIAD1 levels on complex I activity regulation and OXPHOS led us to test whether pharmacological modulation of either would have the same effect on pluripotency and differentiation. Ovarian cancer cells treated with lysophosphatidic acid (LPA) upregulate OCIAD1 (Sengupta et al., 2008). WT
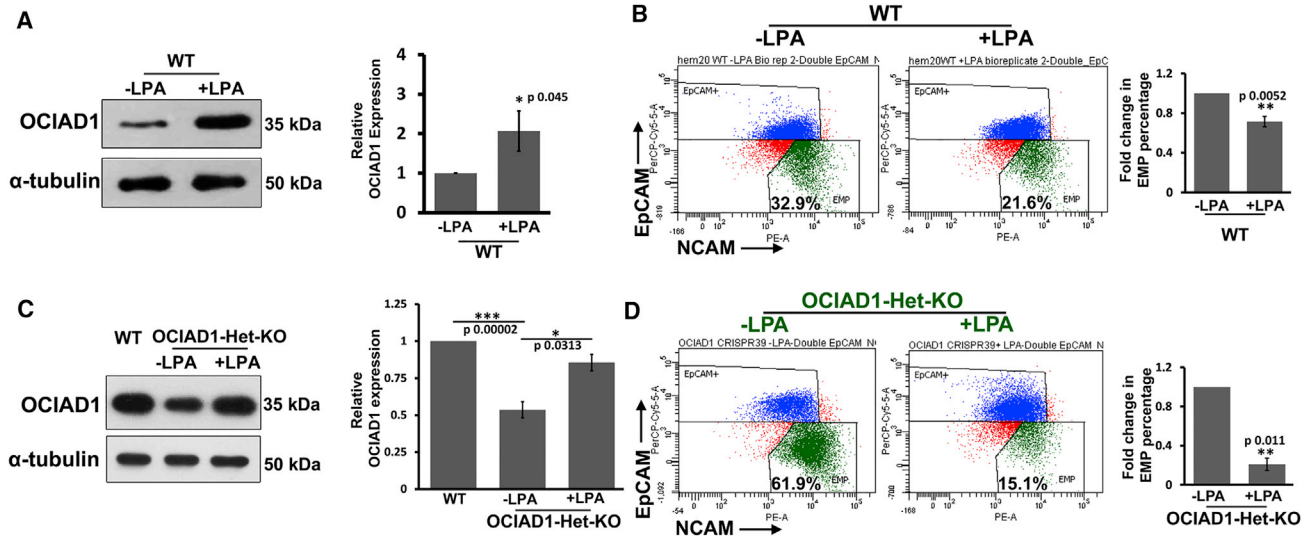
Figure 4. Effect of Pharmacological Enhancement of OCIAD1 Levels on Stem Cell Differentiation

Wild-type (WT), OCIAD1-overexpressing (OV), and OCIAD1-depleted (Het-KO) hESCs were analyzed in the undifferentiated state (A and C) or at day 4.5 of directed mesoderm differentiation (B and D).

(A and B) Effect of LPA treatment on OCIAD1 expression and EMP generation.

(A) Treatment of WT hESCs with 10 μM lysophosphatidic acid (LPA) for 48 hr increased OCIAD1 expression as seen by western blot analysis. Graph represents relative OCIAD1 expression upon LPA treatment (N = 3). Error bars indicate SEM.

(B) LPA-treated WT hESCs show reduced EMP generation in the presence of LPA at day 4.5 as seen by scatterplots of EpCAM and NCAM staining. Graph represents fold changes in EMP percentages compared with WT (N = 3).

(C and D) LPA rescues OCIAD1 depletion phenotype.

(C) Treatment of Het-KO[CRISPR-39] hESCs with 10 μM LPA for 48 hr increased OCIAD1 expression as seen by western blot analysis. Graph represents relative OCIAD1 expression with and without LPA (N = 3).

(D) Het-KO hESCs show reduced EMP generation in the presence of LPA at day 4.5 as seen by scatterplots of EpCAM and NCAM staining. Graph represents fold changes in EMP percentages compared with WT (N = 3).

Error bars show SEM. Statistical significance is indicated by *p < 0.05, **p < 0.01, and ***p < 0.01; NS, not significant.

hESCs cultured in the presence of 10 μM LPA showed a 2-fold increase in OCIAD1 levels (Figure 4A) and a 30% reduction in EMPs generated upon differentiation to day 4.5 (Figure 4B) compared with untreated control cells. Thus, pharmacological increase of OCIAD1 levels also affects EMP generation similar to the OV cells. Conversely, LPA induction of Het-KO cells were able to restore OCIAD1 levels (Figure 4C) and drastically reduced EMP generation (Figure 4D). This suggests that the effect of LPA on EMP generation is likely mediated by OCIAD1. LPA affects multiple signaling pathways and also suppresses Wnt signaling in hESCs (Blauwkamp et al., 2012). OCIAD1 may augment this effect to suppress differentiation.

Pharmacological Modulation of Complex I Activity Allows Control of EMP Generation

We next checked whether targeted pharmacological modulation of complex I activity had similar effects. For this, WT hESCs were cultured in the presence of 10, 15, or 20 μM idebenone, an analog of coenzyme Q that facilitates electron transfer along the respiratory chain. Treatment with

20 μM idebenone increased complex I activity (Figure 5A). Mesendodermal induction of WT and OV hESCs in the presence of 20 μM idebenone resulted in 2.5- and 1.8-fold more EMPs, respectively, compared with untreated cells (Figures 5B and 5C).

To evaluate the outcome of reducing complex I activity on hESC differentiation, we cultured WT and Het-KO hESCs in the presence of 15 nM rotenone, a complex I inhibitor. Partial inhibition of complex I was observed in both the cell lines (Figure 5D). Rotenone treatment of WT as well as Het-KO cells over the period of mesendoderm induction reduced EMP generation at day 3.5 (Figures 5E and 5F), indicating rescue of the Het-KO phenotype caused by reduced OCIAD1 (Figure 5F). Thus, enhanced EMP generation in Het-KO cells could be attributed to an increase in complex I activity. To test whether the EMPs resulting from idebenone-treated hESCs retain their potency, we differentiated them to mesenchymal, endothelial, and cardiac lineages with appropriate protocols (see Experimental Procedures) and found no difference between control and treated hESCs (Figures 5G–5I).
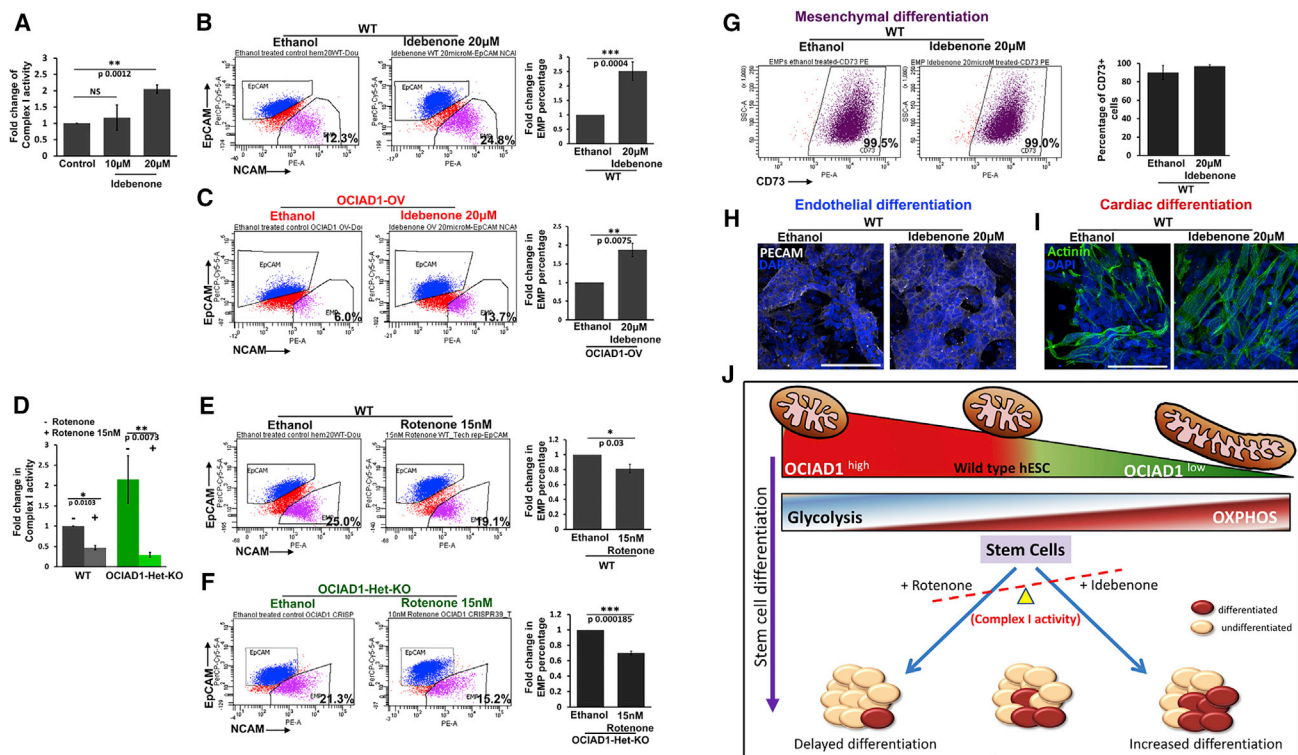
Figure 5. Effect of Modulation of Complex I Activity on Stem Cell Differentiation

Wild-type (WT), OCIAD1-overexpressing (OV), and OCIAD1-depleted (Het-KO) hESCs were analyzed in the undifferentiated state (A and D) or at day 4.5 of directed mesoderm differentiation (B, C, E, and F).

(A–C) Increase in complex I activity enhances EMP specification.

(A) Graph showing fold change in induction of complex I activity in WT hESC lysate in the presence of idebenone (10 μM or 20 μM) (N = 3).

(B) Idebenone-treated (20 μM) WT hESCs show increased EMP generation at day 3.5 as seen by scatterplots of EpCAM and NCAM staining. Graph represents fold changes in EMP percentages compared with WT (N = 3).

(C) OV hESCs show increased EMP generation in the presence of 20 μM idebenone at day 3.5 as seen by scatterplots of EpCAM and NCAM staining. Graph represents fold changes in EMP percentages compared with WT (N = 3).

(D–F) Decrease in complex I activity reduces EMP generation.

(D) Graph showing fold change in inhibition of complex I activity in WT and Het-KO hESC lysate in the presence of 15 nM rotenone (N = 3).

(E) Rotenone-treated (15 nM) WT hESCs show reduced EMP generation at day 3.5 as seen by scatterplots of EpCAM and NCAM staining. Graph represents fold change in EMP percentages (N = 3).

(F) Het-KO [CRISPR-39] hESCs show reduced EMP generation in the presence of 15 nM rotenone at day 3.5 as seen by scatterplots of EpCAM and NCAM staining. Graph represents fold change in EMP percentages (N = 3).

(G–I) Multipotent progenitors derived from idebenone-treated hESCs retain potency. EMPs derived from ethanol (control) or idebenone-treated hESCs differentiated equally well to mesenchyme (expressing CD73, detected by flow cytometry) (G), endothelial (expressing CD31/PECAM detected by immunostaining) (H), and cardiac (expressing actinin detected by immunostaining) (I) lineages as indicated. Scale bars, 100 μm (H) and 50 μm (I).

(J) Schematic depicting the effect of mitochondrial activity on stem cells. Top panel shows the co-relation of OCIAD1 levels with energy metabolic state of hESCs. Bottom half shows the effect of altered mitochondrial ETC complex I activity on stem cell differentiation.

Error bars show SEM. Statistical significance is indicated by $*p < 0.05$, $**p < 0.01$, and $***p < 0.001$; NS, not significant.

In summary, pharmacologically increasing OCIAD1 levels or changing complex I activity levels allows modulation of EMP numbers as expected (Figure 5J); however, their potency is not affected. Hence, we propose that pharmacological increase in complex I activity could serve as a generic method to regulate stem cell differentiation.

DISCUSSION

Elucidating mechanisms that regulate metabolic plasticity of stem cells is a key outstanding problem in stem cell biology. While several regulators of energy metabolism are known, their role in the regulation of stem cell

differentiation is not well investigated. Normal developmental processes are accompanied by change in mitochondrial maturation and activity. However, genetic changes that result in perturbed mitochondrial activity often lead to diseases of impaired metabolism or malignancies (Ghezzi et al., 2011; Swalwell et al., 2011; Tuppen et al., 2010). Thus, identifying additional mechanisms and targets for control of mitochondrial metabolism is important to help devise transient, non-genetic strategies to modulate mitochondrial activity.

We found that human OCIAD1, reported earlier only in the context of carcinomas, is a mitochondrial protein expressed in hPSCs and their differentiated mesodermal derivatives. Furthermore, by genetic modulation of *OCIAD1* we found that its presence aids maintenance of the pluripotent state, whereas reducing OCIAD1 levels promotes hPSC differentiation. This is in agreement with the requirement of *OCIAD1* orthologs in maintaining stem cells in mouse and *Drosophila* (Sinha et al., 2013). Expression analysis indicates that OCIAD1 is present in WT hESCs as well as EMPs. Since OCIAD1-depleted hESCs are pluripotent and form more EMPs, continued expression of OCIAD1 during differentiation of WT hESCs suggests a role in negative regulation of differentiation and/or maintenance of the phenotype. OCIAD1 is likely to function to regulate the energy metabolic state of the cell, possibly by maintaining ETC activity levels. The heterozygous knockout reduces OCIAD1 expression to below 50% and hence impairs control of mitochondrial activity. OCIAD1 is predominantly localized to mitochondria in hPSCs and interacts with a large number of mitochondrial proteins in differentiated (Floyd et al., 2016) and pluripotent cells (Figure 1C). This makes it a promising target for modulating metabolic activity. The lack of physical interaction of OCIAD1 with SDHB, a representative member of complex II, or UQCRC2, a representative of complex III, in hESCs unlike in somatic cells, suggests cell-type-specific interactions with ETC members. This is in agreement with the observation that complex III activity is unperturbed upon modulation of OCIAD1 levels.

To analyze OCIAD1 function, we screened hESC clones to identify homozygous or heterozygous knockouts. It is likely that cells completely depleted of OCIAD1 may not maintain pluripotency. Notably, in over 50 clones tested we could not obtain a homozygous knockout by CRISPR/Cas9 mediated targeting, indicating low frequency of targeting two alleles or the inability of cells to survive or self-renew in the complete absence of OCIAD1. However, heterozygous knockout cells did give a robust phenotype, which is relevant as it represents a possible viable genotype in humans.

PSC expansion, differentiation, and reprogramming methodologies have benefited from culture systems that allow metabolic modulation and offer better control on the outcome of these processes. For example, antimycin A (inhibitor of complex III) supports hPSC propagation by enabling glycolysis to be the prime energy source (Varum et al., 2009). PS48, a small-molecule activator of 3′-phosphoinositide-dependent kinase 1 (PDK1), enhances reprogramming efficiency by generation of a glycolytic intermediate (Zhu et al., 2010). The ability to modulate pluripotency and differentiation metabolically and transiently indicates fluidity of metabolic states in hPSC cultures and possible substates that may be tunable. Slow transition in metabolic profile during iPSC reprogramming suggests that PSCs and differentiated cells exist in different metabolic states, while lineage-specific stem cells and precursors could be in intermediate states (Ito and Suda, 2014). Therefore, delineating mechanisms that regulate the energy metabolic machinery is important for enabling control of stem cell state, fate, and reprogramming.

There is limited understanding of metabolic states in which different types of stem and precursor cells may exist, and the cell intrinsic and extrinsic factors that influence them. Recently, differences in glycolytic rates have also been reported between naive and primed hESCs, indicating that manipulating glycolysis is one way to direct lineage-specific cell fate (Mlody and Prigione, 2016; Popovic and Heindryckx, 2017). We propose that subthreshold increase in mitochondrial oxidative phosphorylation maintains hESCs in a possible substate of pluripotency that is poised for differentiation. Modulating OCIAD1 expression probably shifts the equilibrium of energy metabolism fluxes and tilts the balance in favor of stemness (OV) or against it (Het-KO), the latter supporting differentiation. Thus, OCIAD1 levels could aid in maintaining energy metabolic plasticity. OCIAD1-depleted hPSCs reside in a more oxidative phosphorylation-based energy metabolic state, making the transition to differentiation faster. It remains to be tested whether OCIAD1 overexpression in differentiating precursor cells can promote reversal to pluripotency, which would help in more efficient reprogramming. Our results suggest that normal OCIAD1 levels allow metabolic realignment in stem cell differentiation. Imbalance in OCIAD1 levels pushes the cells to a metabolically less flexible or more committed state (Figure 5J). This also explains why OCIAD1 expression is essential and regulated in hPSCs.

In the presence of LPA, WT hESCs generate fewer EMPs than untreated cells subjected to mesoderm differentiation. However, LPA is known to affect several signaling pathways, and the additive effect of these with OCIAD1 upregulation could lead to reduced EMPs. Hence, we used small-molecule modulators of energy metabolism that allow rapid, reversible, dose-dependent regimens to be

tested for specific outcomes on stem cell fate. Rotenone was used to partially inhibit respiratory complex I activity and affected the ability of hESCs to generate multipotent EMPs. Idebenone, an enhancer of complex I activity, aided efficient early mesodermal specification. Thus, we provide a generic approach for regulating differentiation applicable to PSCs.

While OCIAD1 levels are relatively unchanged during differentiation, our analysis indicates that OCIAD1 levels in the pluripotent state do matter, as they affect differentiation. There is no significant difference in potency of OCIAD1-modulated EMPs for mesodermal lineages such as mesenchyme and hematoendothelium. The role of the protein may be context dependent. Like other pluripotency genes *Oct3/4* and *SOX2*, *OCIAD1* may also have distinct roles in lineage specification and in differentiated cell types (Wang et al., 2012).

The effect mediated by OCIAD1 can be achieved by using LPA, idebenone, or rotenone. While LPA is already a component of Knockout Serum Replacement used in hPSC culture media (Blauwkamp et al., 2012), the use of idebenone or rotenone can now be explored in various stem cell contexts. However, as mentioned earlier, use of these generic molecules will have a ubiquitous and often undesired effect. Identification of specific small-molecule modulators of OCIAD1 level and/or activity should help directed, transient, and reversible changes to the metabolic state to achieve the desired stem cell expansion in a scalable and cost-effective manner.

Our study also suggests that similar mechanisms may operate to actively control energy metabolism during differentiation of various cell types that can now be investigated further. Interestingly, in *Drosophila* and mouse, Asrij/OCIAD1 regulates several additional signaling pathways involved in hematopoiesis and immunity (Khadilkar et al., 2014, 2017; Kulkarni et al., 2011; Sinha et al., 2013). Given the high similarity in functions of Asrij/OCIAD1 in *Drosophila*, mouse, and human stem cells, our study has implications for understanding and monitoring energy metabolic plasticity in several other cell types including cancer cells.

Energy metabolic changes are a significant outcome of aging and cancer. OCIAD1 is upregulated in several carcinomas and reported to promote secondary colony formation in ovarian cancer cell lines (Sengupta et al., 2008; Wang et al., 2010). Reducing OCIAD1 levels or increasing complex I activity could also potentially be used to differentiate cancer cells and slow down the proliferation of carcinoma cells. Thus, our study has uncovered an additional candidate to help screen for anti-cancer drugs. Furthermore, this could directly affect differentiation of cancer cells, stem cell engineering, lineage-specific differentiation, and regenerative medicine. Our study will help

elucidate additional pathways and regulators of energy metabolism in embryonic and adult stem cells, which could help stem cell derivation and reprogramming strategies. As cancer stem cells have an energy metabolic profile similar to that of PSCs, pharmacologically targeting OCIAD1 or its interactors could promote OXPHOS and drive differentiation.

In summary, by experimenting with and using a combination of genetic and non-genetic approaches we have uncovered new ways to help generate multipotent, functional lineage-restricted progenitors by enhancing mitochondrial ETC activity in hESCs. This insight could help improve culture media and differentiation protocols to rapidly generate cells of desired mesodermal lineages for cell replacement therapies. Small-molecule-based modulation of energy metabolic regulation can now also be tested in the context of other stem or progenitor cells of varied potencies.

EXPERIMENTAL PROCEDURES

hESC Culture

The hESC lines BJNhem19 (UKSCB accession no. R-08-022; NIH Stem Cell Registry NIHhESC-10-0083), BJNhem20 (UKSCB accession no. R-08-021; NIH Stem Cell Registry NIHhESC-10-0084) (Inamdar et al., 2009), OCIAD1-OV, OCIAD1-Het-KO[CRISPR-20], and OCIAD1-Het-KO[CRISPR-39] (Shetty and Inamdar, 2016a, 2016b, 2016c) were cultured as described previously (see Supplemental Experimental Procedures).

Proximity Ligation Assay

Semiconfluent cultures of BJNhem20 grown on Matrigel-coated coverslip dishes were fixed in 2% paraformaldehyde, washed, permeabilized with 0.1% Triton X-100 (Sigma-Aldrich), and blocked using 4% fetal bovine serum in a humid chamber at 37°C incubator for 1 hr. Primary antibodies raised against OCIAD1, NDUFS3, MIC60, or Rab4 (negative control) were used in dilution of 1:300 (see Table S2) and incubated at 37°C for 2 hr. Duolink *in situ* PLA reaction (Olink Biosciences, Sigma-Aldrich) was carried out as per manufacturer's instructions. PLA complexes (spots larger than 0.5 μm) were imaged using a Zeiss LSM 880 confocal microscope and counted in 100 cells.

Enzyme Activity Assay of Respiratory Supercomplexes

Activities of respiratory chain complexes I, III, IV, and citrate synthase were measured from whole-cell lysates at 37°C using a microplate reader VersaMax (Molecular Devices) as detailed in Spinazzi et al. (2012) (see Supplemental Experimental Procedures).

Oxygen Consumption Rate and Extracellular Acidification Rate Analysis

hESCs were seeded 48 hr before the experiment onto an XFe24 Cell Culture Microplate (Seahorse Bioscience) at 20,000 cells/well in mTESR1 medium with ROCK inhibitor and incubated at 37°C

overnight, after which medium was changed to −ROCK inhibitor. Cell metabolic-flux rates were measured using an XFe24 Extracellular Flux Analyzer (Seahorse Bioscience) in unbuffered DMEM (XF Base Medium) with Glutamax. Substrates and inhibitors were injected during the measurements at final concentrations of 25 μM glucose, 1 μM oligomycin, and 50 μM 2-DG for ECAR and 0.3 μM FCCP, 1 μM oligomycin, 1 μM rotenone, 1 μM antimycin A for OCR. Three-minute measurement cycles were used. The OCR and ECAR values were normalized to relative viable cells present in each well, quantified using Prestoblue (Thermo Fisher Scientific).

Lysophosphatidic Acid Induction

hESCs cultured on Matrigel were treated with 10 μM LPA (Sigma-Aldrich) or equal volume of solvent DMSO for 48 hr. Cells were harvested, lysed, and probed for OCIAD1 expression by immunoblotting. For analysis of EMP generation upon LPA treatment, WT or Het-KO hESCs were seeded for mesoderm induction. At day 2 when the medium was changed from mTESR1 to Stemline II with growth factors (Stemline II + ABVF), 10 μM LPA or equal volume of DMSO was added to the medium. The medium was changed every 48 hr till the point of analysis at day 4.5.

Complex I Activity Modulation in hESCs

WT or Het-KO hESCs were seeded for mesoderm induction. At 30%–40% confluence (48 hr), desired concentration of rotenone (15 nM) or idebenone (10, 15, or 20 μM) or solvent (ethanol) was added to mTESR1 medium with β-ME. After 36 hr the medium was changed to mesoderm induction medium Stemline II with growth factors (ABVF) + β-ME with rotenone or idebenone/DMSO. The medium was changed every 48 hr until day 3.5. Flow-cytometry analysis of EMPs generated was done at day 3.5 of induction. MnTBAP (50 μM; Calbiochem) was used to quench ROS generated upon rotenone treatment of hESCs.

Statistics

Data are presented as mean ± SEM calculated from three independent experiments. ANOVA or Student's t test (when fold changes were compared) were used for statistical significance analysis.

Further details of hESC culture, enzyme activity assay of respiratory supercomplexes, immunostaining, RNA isolation, qRT-PCR, proliferation analysis, MitoTracker co-localization, live MitoTracker imaging and quantitation, western blotting, and co-immunoprecipitation (coIP) are given in Supplemental Experimental Procedures.

SUPPLEMENTAL INFORMATION

Supplemental Information includes Supplemental Experimental Procedures, six figures, two tables, and one video can be found with this article online at https://doi.org/10.1016/j.stemcr.2018.05.015.

AUTHOR CONTRIBUTIONS

Conceptualized project: D.K.S. and M.S.I.; designed, performed, and analyzed experiments: D.K.S., K.P.K., and M.S.I.; wrote manuscript: D.K.S. and M.S.I.

REFERENCES

Abidari, J.M., Gonzales, E.T., Inoue, K., Lupski, J.R., Karsenty, G., and Katsanis, N. (2000). Identification of novel genes expressed during metanephric induction through single-cell library screening. Kidney Int. *57*, 2221–2228.

Blauwkamp, T.A., Nigam, S., Ardehali, R., Weissman, I.L., and Nusse, R. (2012). Endogenous Wnt signalling in human embryonic stem cells generates an equilibrium of distinct lineage-specified progenitors. Nat. Commun. *3*, 1070.

Calvo, S.E., Clauser, K.R., and Mootha, V.K. (2015). MitoCarta2.0: an updated inventory of mammalian mitochondrial proteins. Nucleic Acids Res. *44*, D1251–D1257.

De Marchi, T., Kuhn, E., Dekker, L.J., Stingl, C., Braakman, R.B., Opdam, M., Linn, S.C., Sweep, F.C., Span, P.N., Luider, T.M., et al. (2016). Targeted MS assay predicting tamoxifen resistance in estrogen-receptor-positive breast cancer tissues and sera. J. Proteome Res. *15*, 1230–1242.

Evseenko, D., Zhu, Y., Schenke-Layland, K., Kuo, J., Latour, B., Ge, S., Scholes, J., Dravid, G., Li, X., MacLellan, W.R., et al. (2010). Mapping the first stages of mesoderm commitment during differentiation of human embryonic stem cells. Proc. Natl. Acad. Sci. USA *107*, 13742–13747.

Floyd, Brendan J., Wilkerson, Emily M., Veling, Mike T., Minogue, Catie E., Xia, C., Beebe, Emily T., Wrobel, Russell L., Cho, H., Kremer, Laura S., Alston, Charlotte L., et al. (2016). Mitochondrial protein interaction mapping identifies regulators of respiratory chain function. Mol. Cell *63*, 621–632.

Ghezzi, D., Arzuffi, P., Zordan, M., Da Re, C., Lamperti, C., Benna, C., D'Adamo, P., Diodato, D., Costa, R., Mariotti, C., et al. (2011). Mutations in TTC19 cause mitochondrial complex III deficiency and neurological impairment in humans and flies. Nat. Genet. *43*, 259–263.

Guarani, V., Paulo, J., Zhai, B., Huttlin, E.L., Gygi, S.P., and Harper, J.W. (2014). TIMMDC1/C3orf1 functions as a membrane-embedded mitochondrial Complex I assembly factor through association with the MCIA complex. Mol. Cell. Biol. *34*, 847–861.

Havugimana, Pierre C., Hart, G.T., Nepusz, T., Yang, H., Turinsky, Andrei L., Li, Z., Wang, Peggy I., Boutz, Daniel R., Fong, V., Phanse, S., et al. (2012). A census of human soluble protein complexes. Cell *150*, 1068–1081.

Inamdar, M.S., Venu, P., Srinivas, M.S., Rao, K., and VijayRaghavan, K. (2009). Derivation and characterization of two sibling human embryonic stem cell lines from discarded grade III embryos. Stem Cells Dev. *18*, 423–434.

International Stem Cell Initiative, Amps, K., Andrews, P.W., Anyfantis, G., Armstrong, L., Avery, S., Baharvand, H., Baker, J., Baker, D., Munoz, M.B., et al. (2011). Screening ethnically diverse human embryonic stem cells identifies a chromosome 20 minimal amplicon conferring growth advantage. Nat. Biotechnol. *29*, 1132–1144.

Ito, K., and Suda, T. (2014). Metabolic requirements for the maintenance of self-renewing stem cells. Nat. Rev. Mol. Cell Biol. *15*, 243–256.

Ji, A.R., Ku, S.Y., Cho, M.S., Kim, Y.Y., Kim, Y.J., Oh, S.K., Kim, S.H., Moon, S.Y., and Choi, Y.M. (2010). Reactive oxygen species enhance differentiation of human embryonic stem cells into mesendodermal lineage. Exp. Mol. Med. *42*, 175–186.

Khadilkar, R.J., Ray, A., Chetan, D.R., Sinha, A.R., Magadi, S.S., Kulkarni, V., and Inamdar, M.S. (2017). Differential modulation of the cellular and humoral immune responses in Drosophila is mediated by the endosomal ARF1-Asrij axis. Sci. Rep. *7*, 118.

Khadilkar, R.J., Rodrigues, D., Mote, R.D., Sinha, A.R., Kulkarni, V., Magadi, S.S., and Inamdar, M.S. (2014). ARF1-GTP regulates Asrij to provide endocytic control of Drosophila blood cell homeostasis. Proc. Natl. Acad. Sci. USA *111*, 4898–4903.

Kulkarni, V., Khadilkar, R.J., Magadi, S.S., and Inamdar, M.S. (2011). Asrij maintains the stem cell niche and controls differentiation during *Drosophila* lymph gland hematopoiesis. PLoS One *6*, e27667.

Kumar, N., Richter, J., Cutts, J., Bush, K.T., Trujillo, C., Nigam, S.K., Gaasterland, T., Brafman, D., and Willert, K. (2015). Generation of an expandable intermediate mesoderm restricted progenitor cell line from human pluripotent stem cells. Elife *4*, e08413.

Li, Y., Park, J.-S., Deng, J.-H., and Bai, Y. (2006). Cytochrome c oxidase subunit IV is essential for assembly and respiratory function of the enzyme complex. J. Bioenerg. Biomembr. *38*, 283–291.

Maraldi, T., Angeloni, C., Giannoni, E., and Sell, C. (2015). Reactive oxygen species in stem cells. Oxid. Med. Cell. Longev. *2015*, 159080.

Mlody, B., and Prigione, A. (2016). A glycolytic solution for pluripotent stem cells. Cell Stem Cell *19*, 419–420.

Mukhopadhyay, A., Das, D., and Inamdar, M.S. (2003). Embryonic stem cell and tissue-specific expression of a novel conserved gene, asrij. Dev. Dyn. *227*, 578–586.

Pagliarini, D.J., Calvo, S.E., Chang, B., Sheth, S.A., Vafai, S.B., Ong, S.-E., Walford, G.A., Sugiana, C., Boneh, A., Chen, W.K., et al. (2008). A mitochondrial protein compendium elucidates complex I disease biology. Cell *134*, 112–123.

Popovic, M., and Heindryckx, B. (2017). Metabolic plasticity complements the unique nature and demands of distinct pluripotency states. Stem Cell Investig. *4*. https://doi.org/10.21037/sci.2017.01.03.

Sengupta, S., Michener, C.M., Escobar, P., Belinson, J., and Ganapathi, R. (2008). Ovarian cancer immuno-reactive antigen domain containing 1 (OCIAD1), a key player in ovarian cancer cell adhesion. Gynecol. Oncol. *109*, 226–233.

Shetty, D.K., and Inamdar, M.S. (2016a). Generation of a heterozygous knockout human embryonic stem cell line for the OCIAD1 locus using CRISPR/CAS9 mediated targeting: BJNhem20-OCIAD1-CRISPR-20. Stem Cell Res. *16*, 207–209.

Shetty, D.K., and Inamdar, M.S. (2016b). Generation of a heterozygous knockout human embryonic stem cell line for the OCIAD1 locus using CRISPR/CAS9 mediated targeting: BJNhem20-OCIAD1-CRISPR-39. Stem Cell Res. *16*, 308–310.

Shetty, D.K., and Inamdar, M.S. (2016c). Generation of transgenic human embryonic stem cell line BJNhem20-OCIAD1-OV. Stem Cell Res. *16*, 192–194.

Sinha, A., Khadilkar, R.J., S, V.K., Roychowdhury Sinha, A., and Inamdar, M.S. (2013). Conserved regulation of the Jak/STAT pathway by the endosomal protein asrij maintains stem cell potency. Cell Rep. *4*, 649–658.

Spinazzi, M., Casarin, A., Pertegato, V., Salviati, L., and Angelini, C. (2012). Assessment of mitochondrial respiratory chain enzymatic activities on tissues and cultured cells. Nat. Protoc. *7*, 1235.

Swalwell, H., Kirby, D.M., Blakely, E.L., Mitchell, A., Salemi, R., Sugiana, C., Compton, A.G., Tucker, E.J., Ke, B.-X., Lamont, P.J., et al. (2011). Respiratory chain complex I deficiency caused by mitochondrial DNA mutations. Eur. J. Hum. Genet. *19*, 769–775.

Tuppen, H.A.L., Blakely, E.L., Turnbull, D.M., and Taylor, R.W. (2010). Mitochondrial DNA mutations and human disease. Biochim. Biophys. Acta *1797*, 113–128.

Varum, S., Momcilovic, O., Castro, C., Ben-Yehudah, A., Ramalho-Santos, J., and Navara, C.S. (2009). Enhancement of human embryonic stem cell pluripotency through inhibition of the mitochondrial respiratory chain. Stem Cell Res. *3*, 142–156.

Varum, S., Rodrigues, A.S., Moura, M.B., Momcilovic, O., Easley, C.A.t., Ramalho-Santos, J., Van Houten, B., and Schatten, G. (2011). Energy metabolism in human pluripotent stem cells and their differentiated counterparts. PLoS One *6*, e20914.

Venu, P., Chakraborty, S., and Inamdar, M.S. (2010). Analysis of long-term culture properties and pluripotent character of two sibling human embryonic stem cell lines derived from discarded embryos. In Vitro Cell. Dev. Biol. Anim. *46*, 200–205.

Wanet, A., Arnould, T., Najimi, M., and Renard, P. (2015). Connecting mitochondria, metabolism, and stem cell fate. Stem Cells Dev. *24*, 1957–1971.

Wang, C., Michener, C.M., Belinson, J.L., Vaziri, S., Ganapathi, R., and Sengupta, S. (2010). Role of the 18:1 lysophosphatidic acid–ovarian cancer immunoreactive antigen domain containing 1 (OCIAD1)-integrin axis in generating late-stage ovarian cancer. Mol. Cancer Ther. *9*, 1709–1718.

Wang, Z., Oron, E., Nelson, B., Razis, S., and Ivanova, N. (2012). Distinct lineage specification roles for NANOG, OCT4, and SOX2 in human embryonic stem cells. Cell Stem Cell *10*, 440–454.

Xu, X., Duan, S., Yi, F., Ocampo, A., Liu, G.H., and Izpisua Belmonte, J.C. (2013). Mitochondrial regulation in pluripotent stem cells. Cell Metab. *18*, 325–332.

Yang, A.H., Chen, J.Y., Lee, C.H., and Chen, J.Y. (2012). Expression of NCAM and OCIAD1 in well-differentiated thyroid carcinoma: correlation with the risk of distant metastasis. J. Clin. Pathol. *65*, 206–212.

Zhang, J., Khvorostov, I., Hong, J.S., Oktay, Y., Vergnes, L., Nuebel, E., Wahjudi, P.N., Setoguchi, K., Wang, G., Do, A., et al. (2011). UCP2 regulates energy metabolism and differentiation potential of human pluripotent stem cells. EMBO J. *30*, 4860–4873.

Zhu, S., Li, W., Zhou, H., Wei, W., Ambasudhan, R., Lin, T., Kim, J., Zhang, K., and Ding, S. (2010). Reprogramming of human primary somatic cells by OCT4 and chemical compounds. Cell Stem Cell *7*, 651–655.